Advances in Geo-Energy Research

Vol. 20, No. 2, p. 145-162, 2026

Original article

# Thermo-hydro-chemical coupled numerical modeling of hydrogen-thermal co-development in hydraulically fractured peridotite

Jiacheng Dai[1,2], Zhonglin Ma[1,2], Yunzhi Yue[1,2], Yujie Yuan[3], Shouceng Tian[1,2]*

[1]*Xinjiang Key Laboratory of Intelligent Oil and Gas Exploration and Development, China University of Petroleum-Beijing at Karamay, Karamay 834000, P. R. China*

[2]*State Key Laboratory of Petroleum Resources and Engineering, China University of Petroleum, Beijing 102249, P. R. China*

[3]*School of Engineering, Edith Cowan University, Joondalup WA 6027, Australia*

**Keywords:**
Thermo-hydro-chemical coupled
numerical model
hydrogen-thermal co-development
serpentinization
sensitivity analysis

**Cited as:**
Dai, J., Ma, Z., Yue, Y., Yuan, Y., Tian, S. Thermo-hydro-chemical coupled numerical modeling of hydrogen-thermal co-development in hydraulically fractured peridotite. Advances in Geo-Energy Research, 2026, 20(2): 145-162.
https://doi.org/10.46690/ager.2026.05.04

**Abstract:**
Hydrogen generation through serpentinization reactions in peridotite formations under high temperature conditions represents a promising avenue for subsurface hydrogen production. However, the thermal energy in the formation environment have not been sufficiently considered. To integrate hydrogen production with thermal energy development, this study develops a thermo-hydro-chemical coupled numerical model, which is used to investigate hydrogen-thermal co-development in hydraulically fractured peridotite. Given that the hydrogen-thermal co-development process involves fluid flow, heat transfer and serpentinization reactions, the governing equations are formulated based on Darcy flow and energy conservation equations, with serpentinization kinetics incorporated through the reactive source terms. To evaluate hydrogen production and thermal energy recovery under varying formation and injection fluid temperatures, the coupled system is solved numerically. The results show that under high geothermal temperature conditions, continuous high-temperature injection combined with moderate natural fracture development can sustain stable high production during long-term operation. When the contribution of thermal energy is neglected, the total system energy output decreases significantly, highlighting the necessity of hydrogen-thermal co-development. This study further identifies the optimal injection temperature range under high geothermal conditions. Under normal geothermal conditions, hydrogen production is limited by reaction temperature, and high-level production cannot be maintained solely through thermal stimulation. Sensitivity analysis reveals that reaction kinetics are the dominant factor controlling system hydrogen productivity, and enhancing them can increase hydrogen production by nearly an order of magnitude. This work establishes a quantitative framework for artificial hydrogen generation and provides theoretical guidance for engineering design and the operational parameter optimization of hydrogen-thermal co-development systems.

## 1. Introduction

Achieving net-zero emissions requires scalable low-carbon energy carriers. To this end, hydrogen is widely regarded as an important complement to electrification and geothermal development (Nadaleti et al., 2021; Gabriel et al., 2022; Hsieh et al., 2024; Manfredi et al., 2026). However, current conventional hydrogen production methods are constrained by

Yandy Scientific Press

*Corresponding author.
*E-mail address*: daijc@cupk.edu.cn (J. Dai); mzl@cupk.edu.cn (Z. Ma); 2025310193@student.cup.edu.cn (Y. Yue); y.yuan@ecu.edu.au (Y. Yuan); tscsydx@163.com (S. Tian).

Received March 11, 2026; revised April 13, 2026; accepted April 30, 2026; available online May 3, 2026.

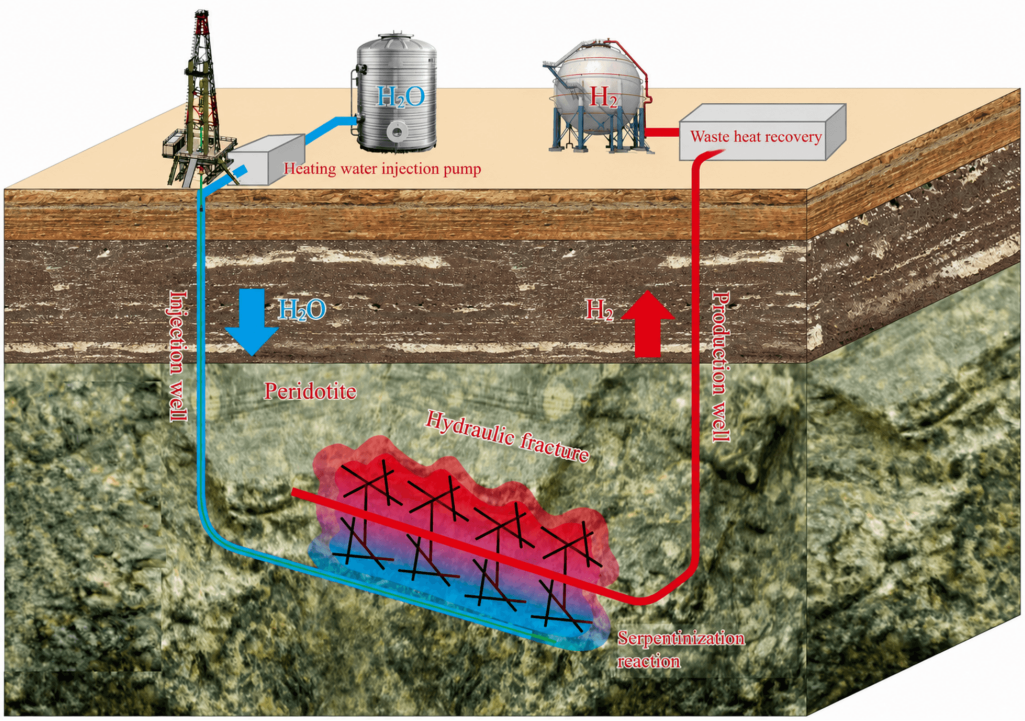


**Fig. 1**. Hydrogen generation from peridotite via hydraulic fracturing in horizontal wells.

high carbon emissions, costs and energy input, as well as deployment limitations, thereby motivating growing interest in geological hydrogen resources and engineered subsurface hydrogen generation (Aliyu and Archer, 2021; Noyan et al., 2023; Vallejo et al., 2024; Zhang et al., 2026).

Natural hydrogen refers to $H_2$ generated in geological structures (Lollar et al., 2014; Zgonnik, 2020). Among the proposed generation mechanisms, the serpentinization of Fe(II)-bearing ultramafic rocks is widely regarded as the primary source of natural hydrogen (Jackson et al., 2024; Wang et al., 2026). The Bourakebougou hydrogen accumulation in Mali is the best documented field example, and broader assessments suggest a substantial global resource base (Prinzhofer et al., 2018; Brandt, 2023). Nevertheless, commercial development relies on a complete generation-migration-accumulation process. Hydrogen generation through serpentinization is limited by reaction rate and reactant availability, which are strongly influenced by temperature, water supply, and the degree of water-rock interaction (Okland et al., 2014; McCollom et al., 2016; Zgonnik, 2020; Rezaee, 2025). In addition, the generated hydrogen may be consumed in the subsurface by microorganisms and by reactions with $CO_2$ and oxidized iron-bearing minerals (Foustoukos and Seyfried, 2004; Kelley et al., 2005; McCollom et al., 2016). Subsequent migration is hindered by the high diffusivity of hydrogen and its strong tendency to leak, leading to substantial loss and dilution (Prinzhofer et al., 2019; Moretti et al., 2023). However, recent experiments and molecular simulations showed that water-saturated rocks can slow hydrogen diffusion, and capillary/interfacial effects in water-bearing media may help retard leakage through sealing formations (Liu et al., 2022; Strauch et al., 2023; Arekhov et al., 2024). These findings suggest that hydrogen leakage may be partly mitigated in water-bearing formations. However, such retardation does not by itself guarantee long-term preservation or large-scale accumulation, which still depends on sustained generation, effective migration pathways, and suitable trapping or sealing conditions (Zgonnik et al., 2019).

In response to the above challenges, Osselin et al. (2022) proposed stimulating hydrogen generation by injecting water into fractured peridotite. Recently, field-scale stimulation experiments have been initiated in peridotite formations in Oman to evaluate the feasibility of engineered geological hydrogen generation through water injection. Building on this basis, this study draws on the engineering concepts of enhanced geothermal systems and hydraulically fractured horizontal wells reservoirs to investigate a hydraulically fractured dual horizontal well configuration (Cao et al., 2018; Aliyu and Archer, 2021; Zhao et al., 2022), as shown in Fig. 1. The overall aim is not only to enlarge water-rock contact and accelerate serpentinization but also to circulate heat and recover geothermal energy along with hydrogen. Compared with a scheme based on two fractured vertical wells, horizontal wells provide a longer contact interval within the target peridotite, intersect more induced fractures, enlarge the effective swept volume, and are more favorable for channeling heated fluids and generated hydrogen toward the production well, thereby enhancing concentrated recovery and reducing hydrogen loss during migration (McCollom and Bach, 2009; Li et al., 2016; Mao et al., 2025; Egert et al., 2026).

In such an engineered system, fluid flow, heat transfer and serpentinization kinetics are tightly coupled. Temperature is especially important because hydrogen generation is favored within an intermediate thermal window, while excessively high

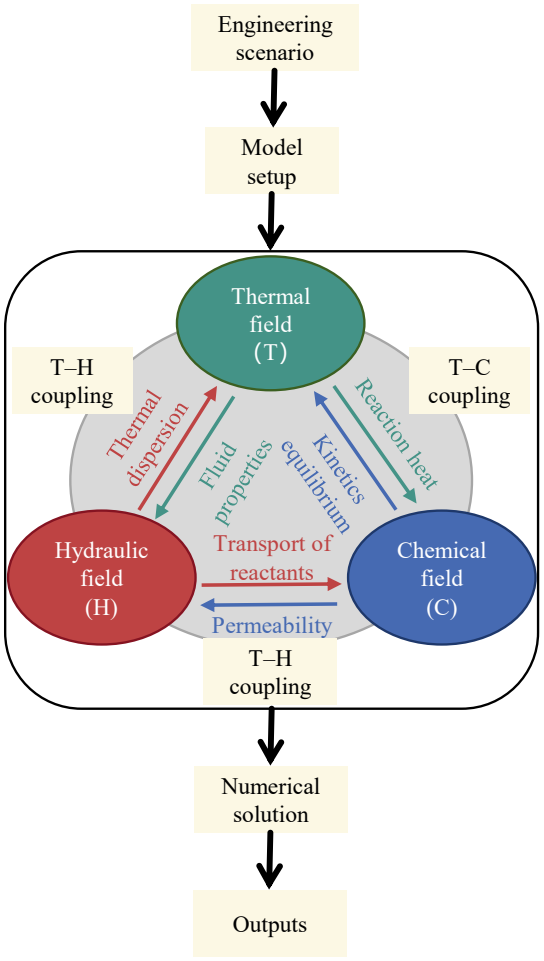


**Fig. 2**. Framework of the THC coupled model.

temperatures suppress continued serpentinization (McCollom and Bach, 2009; McCollom et al., 2016; Huang et al., 2017). The reaction rates are also influenced by mineralogy, pressure and fluid chemistry; previous studies have developed kinetic and thermodynamic frameworks to represent these controls (Allen and Seyfried, 2004; Frost and Beard, 2007; McCollom et al., 2020; Albers et al., 2021). For the present problem, these studies provide the basis for treating serpentinization as a temperature-dependent reactive source term in a reservoir-scale thermo-hydro-chemical (THC) model.

Existing reactive-flow models in geothermal systems, carbonate acidizing, carbon capture, utilization and storage, and petroleum reservoirs demonstrate how heat transfer, fluid flow and chemical reactions can be coupled numerically (Abidoye et al., 2015; Wang et al., 2023; Okere and Sheng, 2025). However, those studies fail to address engineered serpentinization in fractured peridotite, and they do not evaluate hydrogen production together with geothermal heat recovery in a single unified development framework. In contrast, existing natural hydrogen studies have mainly focused on the source mechanisms, reaction kinetics, or exploration-scale migration and accumulation (Kelley et al., 2005; Mügler et al., 2016; Flude et al., 2025). Therefore, studies have insufficiently quantified the feasibility and performance of hydrogen-thermal co-development, in which engineered serpentinization-driven hydrogen generation and geothermal heat recovery are evaluated as an integrated production system. To address this gap, this study establishes a thermal-flow-chemical coupled numerical model for fractured peridotite formations using dual horizontal well and develops a quantitative evaluation framework for hydrogen-thermal co-development. The novelty of this work lies in integrating artificially stimulated serpentinization and geothermal recovery within a unified numerical framework, revealing the influence mechanism of injection temperature on hydrogen-thermal co-production structure, and evaluating the sensitivity of fracture geometry, horizontal well geometry, and reaction kinetic parameters to long-term hydrogen productivity and total system energy output. The results aim to provide a theoretical framework and engineering guidance for the efficient development of artificially stimulated serpentinization hydrogen generation technology via horizontal well fracturing.

## 2. Model establishment

A THC coupled reactive transport model is developed for investigating serpentinization and hydrogen generation induced by artificial water injection in hydraulically fractured peridotite formations. As shown in Fig. 2, the modeling procedure starts from the engineering scenario and model setup, followed by the construction of an integrated THC coupling framework. In this framework, the thermal field, hydraulic field and chemical field are fully coupled through their mutual interactions, including the effects of temperature on flow and reactions, the influence of fluid flow on heat and species transport, and the feedback of chemical reactions on porosity, permeability and fluid properties. The coupled system is then numerically solved, and the resulting model outputs are used to evaluate the spatiotemporal evolution of pressure, temperature, water saturation, hydrogen concentration, hydrogen production, and energy output.

### 2.1 Model assumptions

To describe the coupled fluid flow, serpentinization reaction and heat transfer during artificial hydrogen generation in peridotite under water injection, the following assumptions are adopted:

1) The initial formation is assumed to contain no free water. Serpentinization is initiated only after injected water enters the reactive domain through the wellbore and stimulated fracture network. This assumption reduces the uncertainty related to residual formation water and attributes the onset of hydrogen generation to artificial water injection (Roumejon et al., 2015; Shimizu and Okamoto, 2016).
2) Fluid flow is treated as single-phase water flow, while gas-liquid two-phase flow caused by hydrogen generation is neglected (Mügler et al., 2016). This simplification is appropriate for a first-order thermo-hydro-chemical model focused on the dominant effects of water-rock reaction and heat transfer. Under high-temperature and high-pressure conditions, part of the generated hydrogen may remain dissolved in the aqueous phase. In the simulated cases, the hydrogen concentration is much

lower than its estimated solubility, suggesting that free-gas formation is limited. Therefore, hydrogen generation is represented as an equivalent source term in the single-phase framework. However, this assumption may underestimate the influence of hydrogen exsolution on water mobility and reactive-zone development, especially when gas saturation becomes significant (Boon et al., 2024).

3) A constant water-rock ratio is assumed throughout the production cycle (Malvoisin et al., 2026). This assumption reflects the expectation that, after hydraulic stimulation, the injected fluid volume is much greater than the rock volume involved in the instantaneous reaction, such that water supply remains relatively sufficient. It also signifies the view that temperature, fracture geometry, and reaction kinetics exert stronger first-order controls on hydrogen generation than temporal variations in water-rock ratio. In reality, local water availability may vary because of the reaction consumption, incomplete replenishment and flow heterogeneity, which may jointly affect cumulative hydrogen generation.
4) Hydraulic stimulation is represented by a dominant conductive fracture connected to a surrounding fracture network. The main fracture is assigned a length of 1,400 m, a height of 50 m, and an average aperture of 0.1 mm. These parameters are selected based on reported hydraulic-fracture apertures and constrained vertical fracture growth in enhanced geothermal systems (Davies et al., 2012; Wu et al., 2021). The fracture length of 1,400 m is treated as an engineering assumption representing an extended stimulated flow path after hydraulic fracturing, consistent with field evidence that Enhanced Geothermal System stimulation commonly develops a fracture network rather than a single simple planar fracture (Norbeck et al., 2018). Based on the cubic-law relation for an ideal parallel-plate fracture, an aperture of 0.1 mm corresponds to a permeability of about $8.3 \times 10^{-10}$ $m^2$; considering fracture roughness and stress-induced closure, the effective fracture permeability is taken to be on the order of $10^{-10}$ $m^2$. By contrast, the measured serpentinite permeability is much lower, commonly ranging from $10^{-13}$ to $10^{-20}$ $m^2$, hence the stimulated fracture system is reasonably treated as the principal flow conduit (Hatakeyama et al., 2017; Kottwitz et al., 2020). The fracture permeability is further assumed to remain constant during simulation. This neglects permeability evolution caused by mineral dissolution and precipitation, fracture closure or opening, and stress redistribution. Such processes may influence long-term injectivity, fluid circulation efficiency, and reactive accessibility. As a result, the model may overestimate sustained flow capacity and cumulative hydrogen production where permeability declines over time. Fig. 3 shows that the model was validated against the rock-core experiment of Luhmann et al. (2017) using the same geometry and initial conditions, and acidic fluids such as $NaHSO_4$ can offset permeability loss by promoting dissolution-induced pores and microfractures (Liu et al., 2024).
5) To represent a possible future high-temperature development scenario, rather than a conventional reservoir condition, the 600 °C heated zone is adopted as an idealized local thermal boundary. This assumption is used to explore the behavior of the coupled hydrogen-thermal system under strong thermal support and is broadly aligned with emerging superhot geothermal development goals, such as the Iceland Deep Drilling Project concept of accessing 400-600 °C superheated fluids. Normal geothermal conditions are also considered in Case 3.

Overall, while the assumptions of single-phase flow, constant water-rock ratio, and constant permeability are acceptable for a first-order conceptual model, they may lead to optimistic estimates of injectivity, connectivity and long-term hydrogen productivity. Future work should incorporate gas-liquid multiphase flow, hydrogen exsolution, relative permeability, capillary pressure, gas saturation evolution, and permeability evolution to provide a more realistic assessment of hydrogen migration and recoverability under actual reservoir conditions.

## 2.2 Governing equations

The model describes the coupled processes of fluid flow, heat transfer and reactive transport in a hydraulically stimulated peridotite reservoir, which is represented as a fracture-matrix system. Fluid flow in the porous matrix and hydraulic fractures, heat transport in the rock-fluid system, and Darcy-scale solute transport are all described using standard governing equations commonly applied in fractured porous media and reactive-flow systems (Perez et al., 2013; Mügler et al., 2016; Wang et al., 2021; Mahmoodpour et al., 2022). Since these governing equations were not newly developed in this study, they are not fully presented in the main text. Instead, this section focuses on the reaction-coupling terms that characterize the present model.

In the proposed model, serpentinization affects the thermo-hydraulic system mainly through three coupled mechanisms: Fluid consumption, heat release, and hydrogen generation. The fluid mass sink associated with serpentinization is introduced into the mass conservation equation as:

$$Q = \frac{wR}{\rho_f} \tag{1}$$

where $Q$ represents the fluid mass sink caused by serpentinization, $s^{-1}$; $w$ represents the water-rock ratio; the fluid density $\rho_f$ is calculated by the function $\rho_f = \rho_0[1 - \alpha(T - T_0)]$, $kg/m^3$; $R$ is the serpentinization rate, $kg/m^3 \cdot s$.

The heat released by serpentinization is incorporated into the energy conservation equation as a volumetric heat source term:

$$W = \Delta H R \tag{2}$$

where $W$ represents the heat released by serpentinization, $kJ/m^3 \cdot s$; $\Delta H$ represents the thermal energy released per unit mass of peridotite during the serpentinization reaction, kJ/kg.

Hydrogen generation is treated as a reaction-derived source term linked directly to the serpentinization rate. Under the single-phase assumption adopted in this study, the generated hydrogen is not modeled as a separate gas phase, but its production is accounted for through the reaction source term

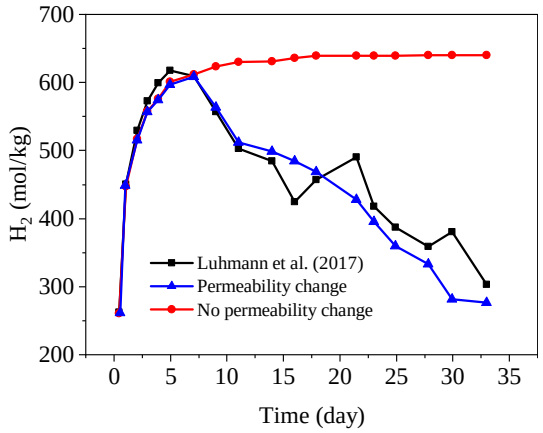


**Fig. 3**. Mathematical model validation.

in the chemical transport framework. In this way, the model captures the first-order coupling between reaction progress, fluid consumption, and thermal evolution while avoiding the unnecessary repetition of standard governing equations.

## 2.3 Serpentinization kinetic equation

Forsterite is the main form of peridotite in many ultrabasic rocks. The reaction rate of serpentinization can be characterized in the form of functions. The starting temperature is about 100 °C and the peak temperature is close to 270 °C. In addition, the reaction rate is also limited by the diffusion of water molecules to the surface of forsterite reaction through the serpentine product layer (Martin and Fyfe, 1970). On this basis, the serpentinization rate equation can be expressed as (Emmanuel and Berkowitz, 2006):

$$R = -\frac{\partial m_r}{\partial t} = K_r m_r \tag{3}$$

where $m_r$ represents the mass of forsterite per unit volume, kg; $t$ represents the reaction time, s; $K_r$ represents the rate constant for the serpentinization reaction, kg/s.

Experimental kinetic data at different temperatures indicate that the rate coefficient $K_r$ can be expressed using a first-order kinetic equation of the following form (Martin and Fyfe, 1970):

$$K_r = A\exp\left[-\alpha(T-T_0)^2\right] \tag{4}$$

where $A$ denotes the serpentinization kinetic parameter, $s^{-1}$; $\alpha$ determines the temperature range of the reaction; $T$ represents the reaction temperature, K; $T_0$ is the temperature at which the serpentinization rate reaches its maximum, K.

Combined with the Avrami kinetic theory, the progress of the serpentinization reaction follows an S-shaped change over time, which can be divided into three stages: Reaction incubation period, acceleration period, and decay period. The Avrami kinetic equation is as follows (Malvoisin et al., 2012):

$$C = 1 - e^{-K_r t^n} \tag{5}$$

where $C$ represents the reaction progress; $n$ is a function of the number and type of time-dependent processes involved in the reaction, with $n = 1$ describing hydration reactions.

In light of the above, this study introduces a reaction progress parameter $C$ to modify the serpentinization rate equation. The modified serpentinization kinetic equation is as follows:

$$R = -\frac{\partial m_r}{\partial t} = K_r m_r (1-C) \tag{6}$$

It should be noted that, although the introduction of the reaction process parameter $C$ can describe the dynamic changes of the serpentinization rate more accurately, the rate equation still cannot fully reflect the complexity of the natural serpentinization process. For example, petrographic observations reveal a complex phenomenon, that is, serpentinization causes the fracturing of peridotite, thus constantly exposing new reaction surfaces (Malvoisin et al., 2012).

## 2.4 Fluid properties and rock composition

In the peridotite formation system, a key element of model construction is the strong dependence of the thermodynamic properties of water (including density, thermal expansion coefficient, compressibility, specific heat capacity, and viscosity) on pressure and temperature. To ensure the simulation accuracy, this paper accurately calculates and characterizes the relevant thermophysical parameters of water based on the standard formula of the International Association for the Properties of Water and Steam (Emmanuel and Berkowitz, 2006). Additionally, the fluid includes components such as $NaHSO_4$ and $NaHCO_3$ to replicate the real formation fluid environment. The rock composition for the numerical simulation is set to a typical peridotite formation, with an initial density of 3,000 $kg/m^3$. Its phase composition consists of 80 wt% peridotite (5.419 mol/kg rock of $Mg_{1.8}Fe_{0.2}SiO_4$), 15 wt% orthopyroxene (1.427 mol/kg rock of $Mg_{0.85}Fe_{0.15}SiO_3$), and 5 wt% clinopyroxene (0.228 mol/kg rock of $CaMg_{0.9}Fe_{0.1}(SiO_3)_2$). This composition is the same as that used by McCollom and Bach (2009).

## 2.5 Model validation

The serpentinization reaction kinetic parameter $A$ is a key parameter controlling hydrogen generation. Although previous studies derived a value of $A = 2\times10^{-6}$ $s^{-1}$ based on serpentinization experiments (Martin and Fyfe, 1970), considering that these experiments were conducted on ground forsterite samples, and the reactive surface area of ultramafic rocks in natural systems is far lower than that of experimental samples, the actual value of $A$ should be several orders of magnitude lower than the experimental one (Malvoisin and Brunet, 2014). Taking these considerations as a basis, the values of the kinetic parameter $A$ and the reaction order $n$ were examined, and the model accuracy in describing the serpentinization process was evaluated by comparing simulations with and without the inclusion of the reaction progress parameter $C$. Values of $A$ in the range of $10^{-9}$ to $10^{-12}$ $s^{-1}$ were explored, with $A$ taken as $5\times10^{-11}$ $s^{-1}$ and $n$ set to 1. The results indicate that, without incorporating C, the simulated reaction behavior shows pronounced deviations from previously published serpentinization experimental data, whereas the inclusion of $C$ enables the model to reasonably reproduce the experimentally observed reaction evolution trends (Marcaillou et al., 2011),

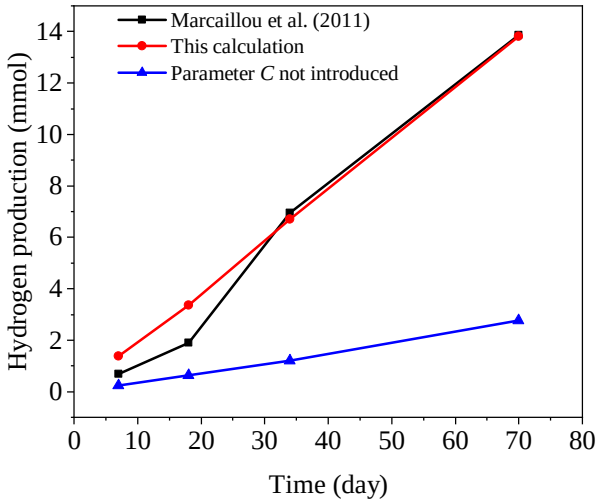


**Fig. 4**. Validation of the serpentinization model.

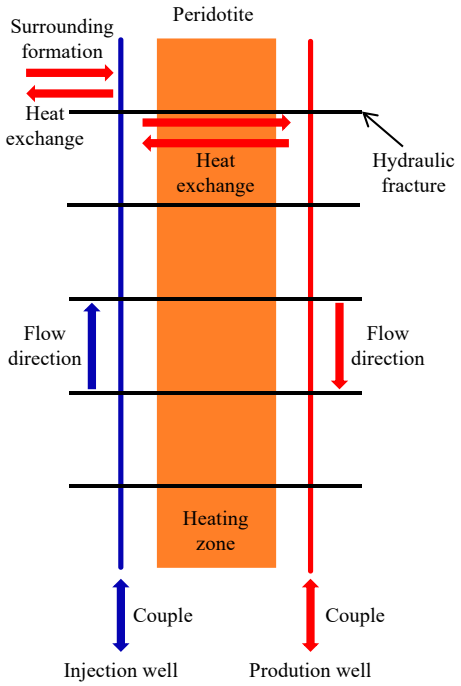


**Fig. 5**. Horizontal-section schematic of the two-dimensional computational model.

as illustrated in Fig. 4.

## 3. A case study of hydrogen generation in fractured peridotite

### 3.1 Computational model

In order to investigate hydrogen generation and heat recovery in a hydraulically stimulated peridotite reservoir, a two-dimensional computational model was established at reservoir depth. This model was designed to represent the main fluid-flow pathway between the injection and production wells, as well as the coupled heat-transfer and serpentinization processes within the fractured reservoir. As shown in Fig. 5,

**Table 1**. Model parameters.

| Parameter | Value |
|---|---|
| Length × Width of the model (m) | 2,000 × 1,500 |
| Horizontal well length (m) | 1,800 |
| Horizontal well diameter (inch) | 7 |
| Well spacing (m) | 700 |
| Length of main fracture (m) | 1,400 |
| Half-length of unconnected hydraulic fracture (m) | 300 |
| Fracture height (m) | 50 |
| Width of hydraulic fracture (mm) | 0.1 |
| Number of fractures (-) | 5 |
| Fracture spacing (m) | 320 |
| Permeability of non-heated zone ($m^2$) | $8 \times 10^{-13}$ |
| Permeability of heated zone ($m^2$) | $10^{-13}$ |
| Temperature of heated zone (°C) | 600 |

the domain consists of a peridotite reservoir, an injection well, a production well, hydraulic fractures between the two wells, and a central heated zone. The injected fluid migrates laterally from the injection well to the production well through the fracture-matrix system, where serpentinization occurs and generates hydrogen along the flow path. Meanwhile, heat is exchanged among the heated zone, the flowing fluid, the hydraulic fractures, and the surrounding formation. This simplified two-dimensional representation captures the main flow, heat-transfer, and reaction characteristics of the stimulated peridotite reservoir while maintaining computational efficiency.

Taking the finite element theory as a basis, this study conducts numerical simulations of serpentinization hydrogen generation in fractured peridotite formations with horizontal wells using COMSOL Multiphysics. This platform achieves a unified description of heat transfer, flow, and chemical reaction processes by solving systems of coupled partial differential equations. To ensure computational stability for large-scale coupled problems, the numerical solution employs a direct solver, and time discretization uses an implicit backward differentiation scheme. Table 1 lists the parameters for the horizontal well model and the fracture model. Some model parameters refer to the settings by Cao et al. (2018) and Zhao et al. (2022), whereas the case-specific settings adopted for Cases 1-3 are summarized in Table 2.

### 3.2 Initial and boundary conditions

The formation system considered in the model primarily consists of peridotite as described in Section 2.3. The formation pressure is 35 MPa, the injection well injects water at a constant pressure of 50 MPa, the initial temperature of the water varies according to different cases, and the outlet pressure of the production well is maintained at 15 MPa. To characterize the hydrogen generation potential under the high

**Table 2**. Summary of the three simulation cases.

| Cases | Geothermal condition | Thermal setting | Injection temperature strategy | Main purpose |
|---|---|---|---|---|
| Case 1 | High geothermal temperature environment | Heated zone included, 600 °C | Continuous high-temperature injection, 230 °C | Evaluate the maximum hydrogen production potential under sufficient geothermal supply |
| Case 2 | High geothermal temperature environment | Same as Case 1; heated zone = 600 °C | Low-temperature injection, 20 °C; additional sensitivity analysis for 20-400 °C | Evaluate the effect of injection temperature on hydrogen generation and hydrogen-thermal energy output structure |
| Case 3 | Normal geothermal environment | No heated zone; formation temperature = 70 °C | Short-term 300 °C thermal activation followed by 20 °C injection after 7 years; compared with continuous 300 °C injection | Assess whether thermal activation can sustain serpentinization and hydrogen production under normal geothermal conditions |

geothermal temperature condition, a heated zone is introduced in the model, with its temperature set to 600 °C, corresponding to a permeability of $10^{-13}$ $m^2$, while the permeability of non-heated zones is $8 \times 10^{-13}$ $m^2$. This temperature does not represent the natural reservoir background temperature but it is an idealized local heat-source condition introduced to explore future development scenarios with strong thermal support. Meanwhile, this study does not focus solely on this high-temperature case, but a normal geothermal condition is also considered in Case 3 to evaluate system behavior under more conventional thermal settings. The above parameter settings are used to depict the heat transfer and reaction characteristics of the fracture-matrix system in high-temperature peridotite formations, sharing the same physical context as the model settings used by Mügler et al. (2016) for simulating the serpentinization hydrogen generation process under the high geothermal temperature condition.

Wellbore-formation heat exchange is described using an infinite line-source model based on Kelvin's theory (Ingersoll et al., 1955). In this treatment, the wellbore is approximated as a line heat source, and the heat transfer between the wellbore and the surrounding formation is described using standard thermal boundary conditions. This simplified approach is adopted to capture the first-order heat-transfer behavior around the wellbore without introducing unnecessary mathematical detail.

## 3.3 Simulation grid

In order to improve the numerical accuracy of the coupled flow, heat-transfer, and reaction simulations, local mesh refinement was applied in regions with strong gradients, including the wells, fractures, and heated zone. The computational grid represents the horizontal-section layout of the model, with the heated zone highlighted in the interwell area for clarity.

In order to ensure that the simulation results are not influenced by the number of grids, this paper studies the produced fluid temperature under different grid numbers. The results indicate that when the number of grid units exceeds about 150,000, the produced fluid temperature tends to stabilize. At the same time, the calculation time increases significantly with the increase in the number of grid units. Therefore, considering the calculation accuracy and efficiency, the grid scheme containing 185,623 grid units was finally selected. Finally, the mathematical equations were solved using a multi-field coupled numerical solution approach.

## 3.4 System production capacity and power evaluation framework

The multi-field coupled system proposed in this study integrates the functions of geothermal recovery and hydrogen production. To quantitatively evaluate the comprehensive energy output efficiency of the system, this paper establishes an evaluation framework based on energy and power. Energy generation primarily originates from two mechanisms. First, system heat recovery mainly depends on the enthalpy difference between the produced fluid and the injected fluid, and its magnitude can be characterized through thermodynamic calculations. This part of the energy change can be calculated using the following formula (Ingersoll et al., 1955; Aliyu and Archer, 2021):

$$Q_w = \frac{M c_w \rho_w \phi (t_r - t_0)}{3600} \tag{7}$$

where $Q_w$ represents the heat generated by the injected water, kWh; M represents the thickness of the thermal reservoir, m (taken as 1 in two-dimensional models); $\phi$ represents the porosity of the thermal reservoir rock, dimensionless; $t_r$ represents the production temperature, °C; $t_0$ represents the injection temperature, °C; $\rho_w$ represents the density of geothermal water, kg/$m^3$; $c_w$ represents the specific heat of water, kJ/(kg·°C).

The second energy source is the hydrogen output, quantified by the calorific value of hydrogen combustion. The calculation formula is as follows (Nadaleti et al., 2021; Gabriel et al., 2022):

$$Q_H = \frac{V_H \rho_H L_{HV}}{3600} \tag{8}$$

where $Q_H$ represents the energy generated by hydrogen com-

bustion, kWh; $V_H$ represents the volume of hydrogen, $m^3$; $\rho_H$ represents the density of hydrogen, $kg/m^3$; $L_{HV}$ represents the lower heating value of hydrogen, kJ/kg, typically 120,000 kJ/kg.

Therefore, the total energy generated by the entire system is calculated as:

$$Q = Q_w + Q_H \tag{9}$$

where $Q$ represents the total energy generated by the entire system, kWh.

Power is defined as the work done or energy converted per unit of time, given by the formula:

$$P = \frac{Q}{t} \tag{10}$$

where $P$ represents the power generated by the system, kW.

In addition to the gross energy output, the thermal energy carried by the injected hot water should be considered, since it represents an external energy input to the system. Therefore, a first-order net energy indicator is introduced to evaluate the influence of hot-water injection on the overall energy performance. The input thermal energy associated with the injected water is calculated as (Aliyu and Archer, 2021):

$$Q_{in} = \frac{M c_w \rho_w \phi (t_0 - t_{ref})}{3600} \tag{11}$$

where $Q_{in}$ represents the thermal energy carried by the injected water, kWh; $t_{ref}$ is the reference temperature, $t_{ref} = 20$ °C.

Then, the net energy output of the system can be expressed as:

$$Q_{net} = Q - Q_{in} \tag{12}$$

where $Q_{net}$ represents the net energy output, kWh.

It should be noted that this net energy indicator is mainly used to assess the effect of thermal energy input from hot-water injection, and as such it remains a first-order energy input-output analysis. Pumping energy consumption, wellbore and surface heat losses, and the energy consumption for hydrogen separation and compression are not fully included, so the results should not be interpreted as a complete system-level net energy or techno-economic evaluation. A more comprehensive energy balance model is still needed in future work.

## 4. Case study

Taking the above thermal-flow-chemical multi-field coupled model as a basis, this chapter analyzes the hydrogen production and energy output characteristics of the system under three typical geothermal environments and operating strategies, and reveals the coupling mechanisms and differences between hydrogen generation and thermal energy recovery processes in different scenarios.

### *4.1 Case 1: High-temperature injection under high geothermal conditions*

Referring to the existing geological backgrounds such as the high-temperature ophiolite environment in the Nagsasa area of the Philippines, geothermal fields in Iceland (Aquino et al., 2025), and the Rainbow hydrothermal field on the Mid-Atlantic Ridge (Mügler et al., 2016), this case constructs a simulation scenario of a deep peridotite reservoir with rich geothermal energy supply. In the geological model, a constant high-temperature heated zone of 600 °C is set up to simulate the heat source supply, so as to ensure that the overlying reservoir is in the background of high heat flow. In this case, the continuous injection of 230 °C high-temperature water is applied as the operating condition. The temperature is within the effective range where serpentinization reaction kinetics are significantly enhanced and mineral phases remain stable, and at the same time, it is also feasible for engineering. This case is used to evaluate the maximum hydrogen production potential of the system under sufficient geothermal energy conditions. To consider the impact of natural fractures on fluid migration and heat exchange processes, this study constructs a two-dimensional discrete natural fracture network model based on the random distribution function. The specific steps are provided in Supplementary *A* of the supplementary information.

In order to examine the effects of natural fractures on flow, heat transfer and hydrogen generation, the pressure distribution, water saturation and hydrogen concentration were analyzed. In the absence of natural fractures, continuous water injection creates a high-pressure zone around the left injection well, while a distinct low-pressure funnel forms near the right production well. The high-pressure area, concentrated near the injection well, expands over time, sustaining the pressure difference and driving fluid flow along the main hydraulic fractures (Fig. 6(a)). Fluid mainly follows these fracture channels, and due to their high conductivity, the injected high-temperature fluid rapidly advances, forming localized high-temperature, high-pressure reaction windows near the wells and main fractures (Fig. 6(b)). When natural fractures are present, these high-permeability pathways provide additional seepage channels, distorting isobaric contours and extending the high-pressure zone along the fracture directions (Fig. 6(e)). The fractures expand fluid migration pathways, allowing water to diverge into multiple routes within the fracture-matrix system. This reduces flow velocity in individual fractures and slows local heating, while it increases the water-rock contact, enhancing heat transfer and serpentinization along the network (Fig. 6(f)). The distributions of water saturation and hydrogen concentration reflect these differences. Without natural fractures, the main hydraulic fracture dominates flow, and water saturation shows a concentrated high-saturation area (Fig. 6(c)). Over time, water diffuses into the surrounding matrix, expanding the high-saturation region and supplying reactants for serpentinization. Hydrogen initially forms at the fracture-matrix interface in the fifth year, then gradually spreads, connecting enrichment zones (Fig. 6(d)). With natural fractures, fluid percolation is significantly enhanced, making water-bearing zones more discrete and widespread. This promotes serpentinization across a larger volume, forming well-connected hydrogen enrichment zones (Figs. 6(g) and 6(h)).

To evaluate the hydrogen production and energy output characteristics of Case 1 over a 20-year production cycle, the hydrogen production rate, cumulative hydrogen production, power, and energy curves for Case 1 over a 20-year production cycle were shown in Fig. 7. The hydrogen production rate

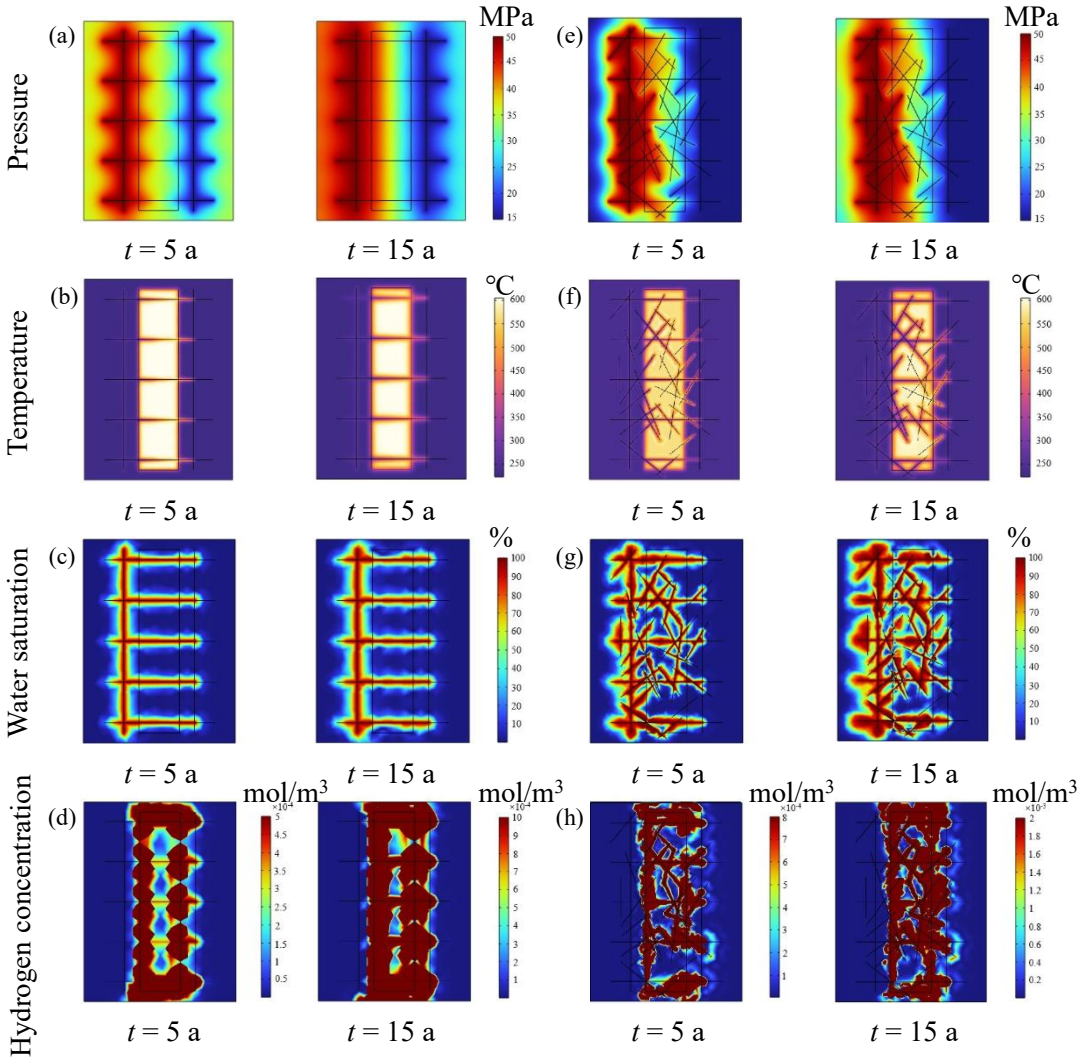


**Fig. 6**. Evolution of pressure, temperature, water saturation, and hydrogen concentration fields in Case 1. (a)-(d) Without natural fractures and (e)-(h) with natural fractures.

curve in the presence of natural fractures (Fig. 7(a)) exhibits distinct three-stage kinetic characteristics:

1) Startup period from year 0 to year 10. In the absence of natural fractures, heat concentrates near the hydraulic fractures, causing a rapid local temperature rise and steep increase in hydrogen production (Fig. 7(a)). When natural fractures are present, the production rises quickly during the first year and gradually levels off from year 2 to year 10 due to fluid diversion, which expands the water-rock contact while slowing local heating. This results in higher power output compared to the fracture-free case (Fig. 7(b)).
2) Acceleration period from year 10 to year 17. Without natural fractures, limited water-rock contact restricts the hydrogen production rate, which stabilizes around 3,000 $m^3$/d. With 100 natural fractures, the expanded contact area accelerates hydrogen generation via Arrhenius-controlled kinetics, reaching a peak of approximately 4,300 $m^3$/d (Fig. 7(a)). During this stage, the cumulative production rises nearly tenfold compared to the fracture-free case.
3) Decay period after year 17. Residual source rock continues to react in the fracture-free scenario, slowly increasing hydrogen production. In contrast, with natural fractures, efficient heat transfer and expanded water-rock contact cause the reaction zone to consume more source rock, leading to a decline in the hydrogen production rate (Fig. 7(a)). Meanwhile, system power (Fig. 7(b)) remain relatively high. It is noteworthy that as the number of natural fractures continues to increase, the improvement in hydrogen production rate tends to level off. This is because an excessive number of fractures intensifies competition for fluid among different channels, which shortens the fluid residence time and limits the duration of water-rock reactions. At the same time, part of the fluid may preferentially flow through highly connected fractures, reducing the effective contact between water

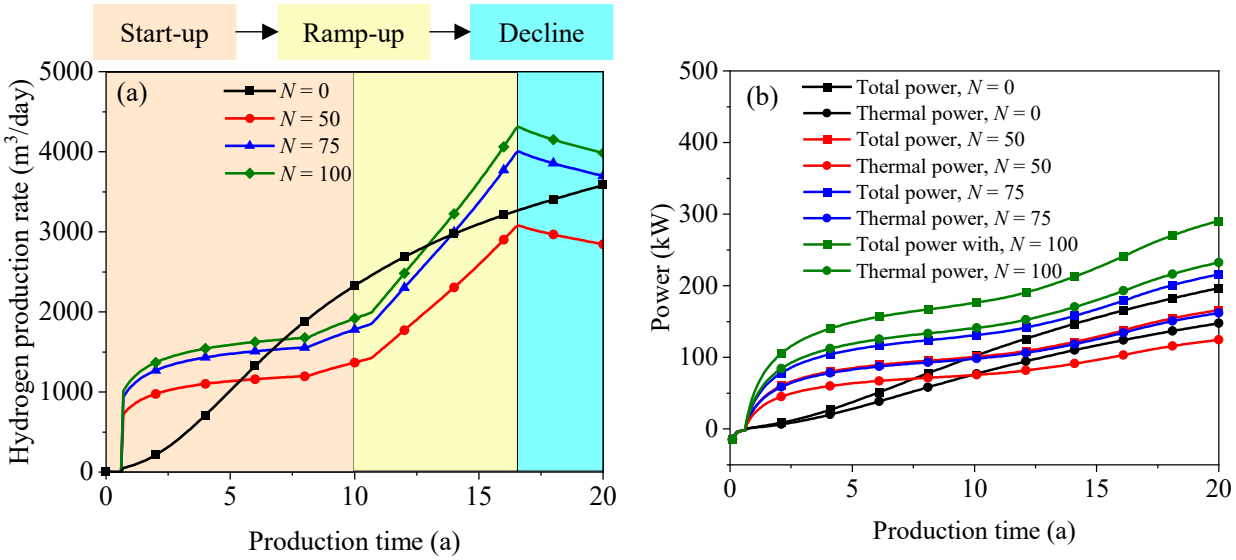


**Fig. 7**. Hydrogen production and energy output in Case 1. (a) Hydrogen production rate and (b) power. (*N* is the number of fractures)

and reactive rock surfaces. Consequently, the additional gain in hydrogen production becomes limited despite the further increase in fracture number. Furthermore, when the number of natural fractures is relatively low (50 natural fractures), due to insufficient reaction rates during the startup period and declining rates during the decay period, the overall hydrogen production efficiency of the system falls below that of the condition without natural fractures. Therefore, to reduce uncertainty in subsequent strategy discussions, the following analyses will exclude natural fractures. To more clearly focus on the influence of formation temperature environment, injection temperature, and parameters on the system, the model will retain only the main hydraulic fractures.

## 4.2 Case 2: Low-temperature injection under high geothermal conditions

This case shares the same geothermal conditions as Case 1, but the injection temperature is adjusted from continuous high-temperature injection to low-temperature water (20 °C) injection. The aim is to compare and analyze the impact of injection temperature changes on the intensity of serpentinization reactions, hydrogen production behavior, and the structure of system energy output, thereby evaluating the synergistic characteristics of hydrogen generation and geothermal energy recovery.

In order to examine the impact of low-temperature injection on system behavior, the evolution of the pressure field, temperature field, water saturation, and hydrogen concentration in Case 2 is analyzed. Under low-temperature injection conditions, the overall characteristics of the pressure field (Fig. 8(a)) and water saturation (Fig. 8(c)) are consistent with Case 1. A high-pressure zone is formed near the injection well and the pressure gradient continuously drives the fluid to the production well along the main fracture. However, since the temperature of the injected fluid is much lower than that of the formation, the cold fluid first absorbs heat from the surrounding rocks near the injection well, establishing a stable temperature gradient near the fracture and gradually expanding in the direction of the main fracture. Although the deep high geothermal temperature environment continuously supplies heat to the fluid, after 15 years of production, the high-temperature zone has expanded compared to the initial stage, but the overall temperature level in the reaction zone remains significantly lower than the high-temperature reaction window in Case 1 (Fig. 8(b)). Constrained by the overall decrease in reaction zone temperature, the intensity of the serpentinization reaction is significantly suppressed. In this case, the hydrogen concentration is reduced by approximately two orders of magnitude compared to Case 1, and the area of the effective reaction zone is also significantly reduced (Fig. 8(d)). This strategy confirms that changes in the injected fluid temperature have a decisive controlling effect on the hydrogen generation behavior.

In order to investigate the influence of injection temperature, simulation results for injection temperatures ranging from 20 to 400 °C were analyzed. As shown in Fig. 9, when the injection temperature is 20 °C, the hydrogen production of the system is significantly lower than the high-temperature injection condition in Case 1. The hydrogen production rate decreases by about 80%, and the cumulative hydrogen production decreases by nearly 85%, indicating that low-temperature injection seriously limits the effective occurrence of the serpentinization reaction. As the injection temperature rises from 20 to 150 °C, the hydrogen production rate of the system shows an upward trend, with a peak increase of nearly four times (Fig. 9(a)), indicating that increasing the injection temperature can effectively enhance the kinetic process of serpentinization. At different injection temperatures, the total power of the system continues to increase with the extension of hydrogen production time, and the higher the injection temperature is, the higher the total power (Fig.

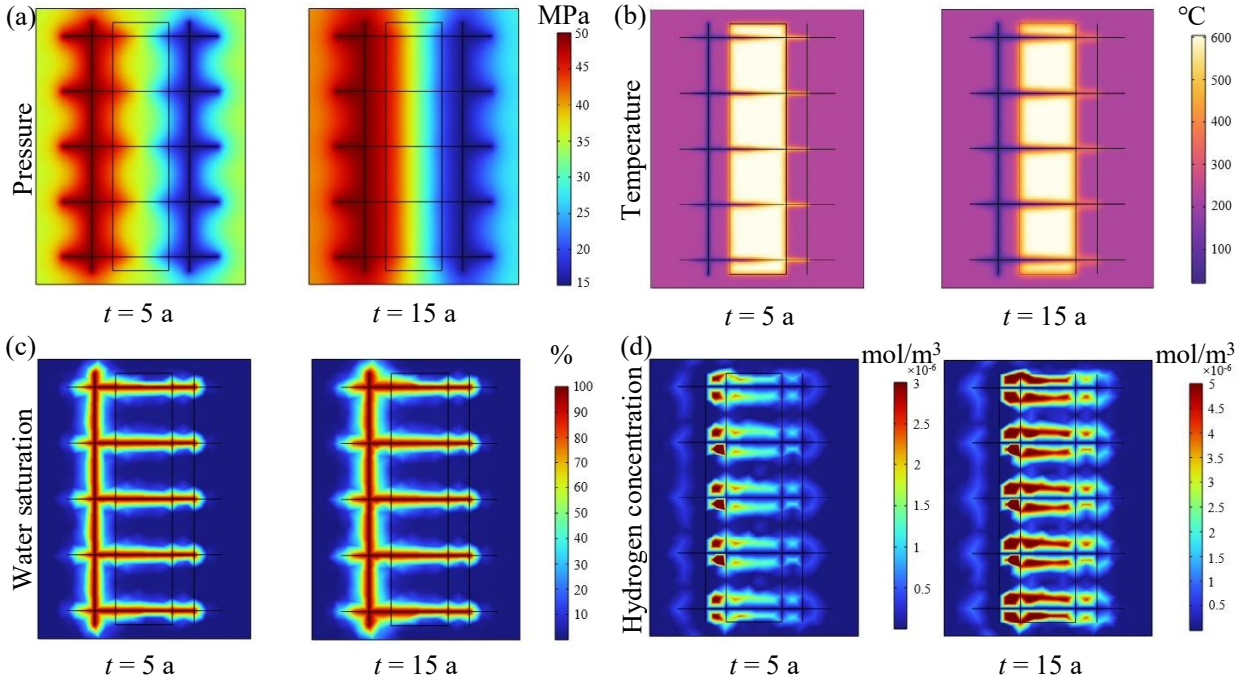


**Fig. 8**. Evolution of pressure, temperature, water saturation, and hydrogen concentration fields in Case 2. (a) Pressure field, (b) formation temperature, (c) water saturation and (d) hydrogen concentration.

9(b)). However, under the injection condition of 20 °C, the proportion of hydrogen energy to the total energy output of the system is relatively low, and the proportion of thermal energy is more than 95%. The energy output of the system is mainly composed of thermal energy. With the injection temperature increasing, although the proportion of hydrogen energy rises, it still does not exceed 20% (Figs. 9(b) and 9(c)). Fig. 9(d) compares the total energy, thermal energy, and input energy. With the injection temperature increasing, both total energy and thermal energy first increase and then decrease, indicating that moderate thermal stimulation enhances serpentinization and heat recovery. However, the input energy increases continuously with injection temperature, leading to a gradual decline in the energy output-to-input ratio. Considering the net total energy, the system shows the highest energy benefit within 230-300 °C. Further increasing the injection temperature requires additional external heat input but does not further improve the total energy output. Therefore, under the first-order energy evaluation framework adopted in this study, the 230-300 °C can be regarded as a favorable injection-temperature range for maximizing the net total energy.

From an engineering perspective, maintaining such an injection temperature range may be feasible when sufficient external or recycled heat sources are available, such as geothermal reinjection heat exchange, industrial waste heat, or heat recovered from the produced fluid. However, the practical implementation should also consider additional energy consumption for water preheating, heat loss during surface transportation, and the thermal resistance of injection equipment. Therefore, the proposed optimal injection temperature range should be regarded as a target operating window that requires heat-source matching and system-level energy balance in practical applications. The energy structure characteristics under this case are closer to a conventional Enhanced Geothermal System, making it suitable as a comprehensive development model primarily focused on geothermal energy recovery with synergistic hydrogen generation.

### 4.3 Case 3: High-temperature activation under normal geothermal conditions

Some ultrabasic rock formations with natural hydrogen development potential are located in normal geothermal temperature environments, such as the peridotite formations in the Oman region, the ophiolite formations in Zambales, Philippines, and Bulqizë, Albania. These occurrences have been documented in previous studies (Aquino et al., 2025). In these settings, the low natural formation temperature and injected ambient-temperature fluid make it difficult to initiate serpentinization, resulting in low hydrogen production for extended periods. Continuous high-temperature injection can enhance reaction intensity but requires substantial external heat and operational costs, limiting economic feasibility. To address these challenges, Case 3 proposes a phased injection scheme of short-term high-temperature activation followed by long-term low-temperature operation. This scheme targets normal geothermal temperature environments (70 °C) where serpentinization reactions are difficult to initiate naturally. It designs a short-term injection of 300 °C high-temperature water for thermal activation, switching to 20 °C low-temperature water injection at the seventh year to assess the sustainability of the activated reaction. Additionally, it explores the impact of continuous injection of 300 °C high-temperature water on the system.

In order to investigate the effects of short-term high-

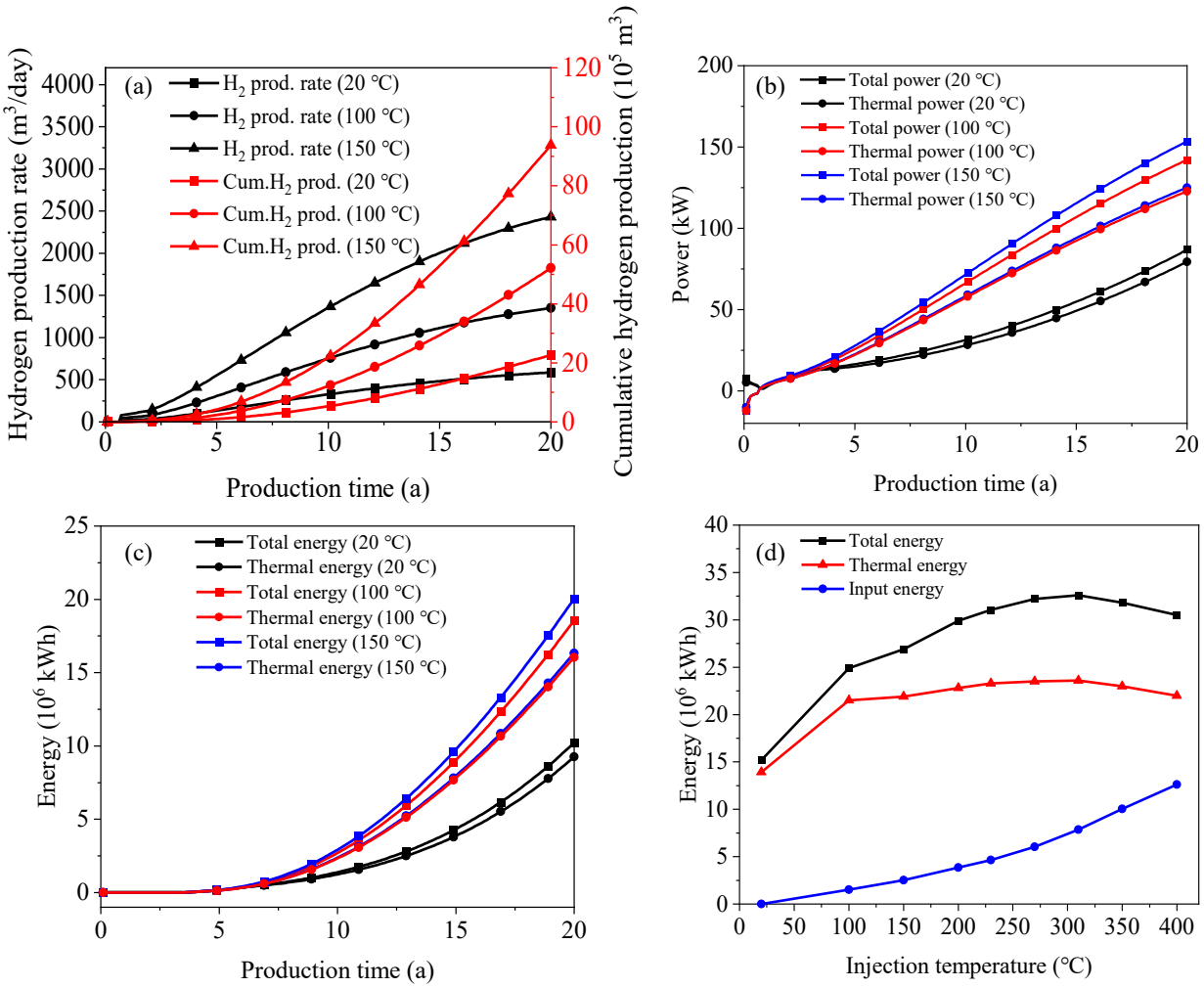


**Fig. 9**. Effects of injection temperature on hydrogen production and energy output in Case 2. (a) Hydrogen production rate and cumulative hydrogen production, (b) power output, (c) energy output and (d) energy variation with injection temperature.

temperature activation and continuous high-temperature injection on the formation, the evolution of temperature, water saturation and hydrogen concentration in Case 3 are analyzed. During the short-term high-temperature activation, the injected fluid rapidly heats the formation near the injection well and along the main fracture, while temperature decays quickly along the fracture, preventing a large-scale high-temperature zone. After switching to low-temperature water after 7 years, temperatures near the injection well drop below the formation temperature, forming a distinct cooling zone. Reaction heat from serpentinization is rapidly dissipated, causing the reaction rate to fall sharply and the cessation of new hydrogen-rich zones forming; existing hydrogen mainly originates from the earlier activation phase. In contrast, under the continuous high-temperature injection strategy, the high-temperature fluid migrates stably along the main fracture. Although the diffusion range of the high-temperature zone is limited, and the high-temperature zone can maintain a higher temperature for a long time near the injection well and the fracture vicinity. With the extension of operating time, the high-temperature fluid gradually diffuses along the main fracture and the hydrogen-rich zone continues to expand, forming a wide, thick and continuous hydrogen production belt.

In order to evaluate hydrogen production and energy output under short-term high-temperature activation and continuous high-temperature injection in Case 3, the hydrogen production rate, cumulative hydrogen production, power, and energy curves over the 20-year production cycle are analyzed. During the short-term high-temperature activation phase (Figs. 10(a) and 10(b)), hydrogen production first rises rapidly but declines sharply after switching to low-temperature injection, with a secondary peak due to exothermic serpentinization feedback. In the normal geothermal environment, heat is quickly lost, limiting the reaction and causing cumulative hydrogen production to plateau (Fig. 10(a)). After 7 years, hydrogen output decreases, and thermal energy dominates system output (Fig. 10(b)), showing that periodic external heating alone cannot sustain long-term reactions. Continuous high-temperature injection maintains hydrogen production (Fig. 10(c)), but the rates and cumulative production remain far below Case 1. The total system energy is negative (Fig. 10(d)), indicating high external energy demand with limited hydrogen output. These results suggest that economically viable hydrogen production is challenging under normal geothermal conditions. Future

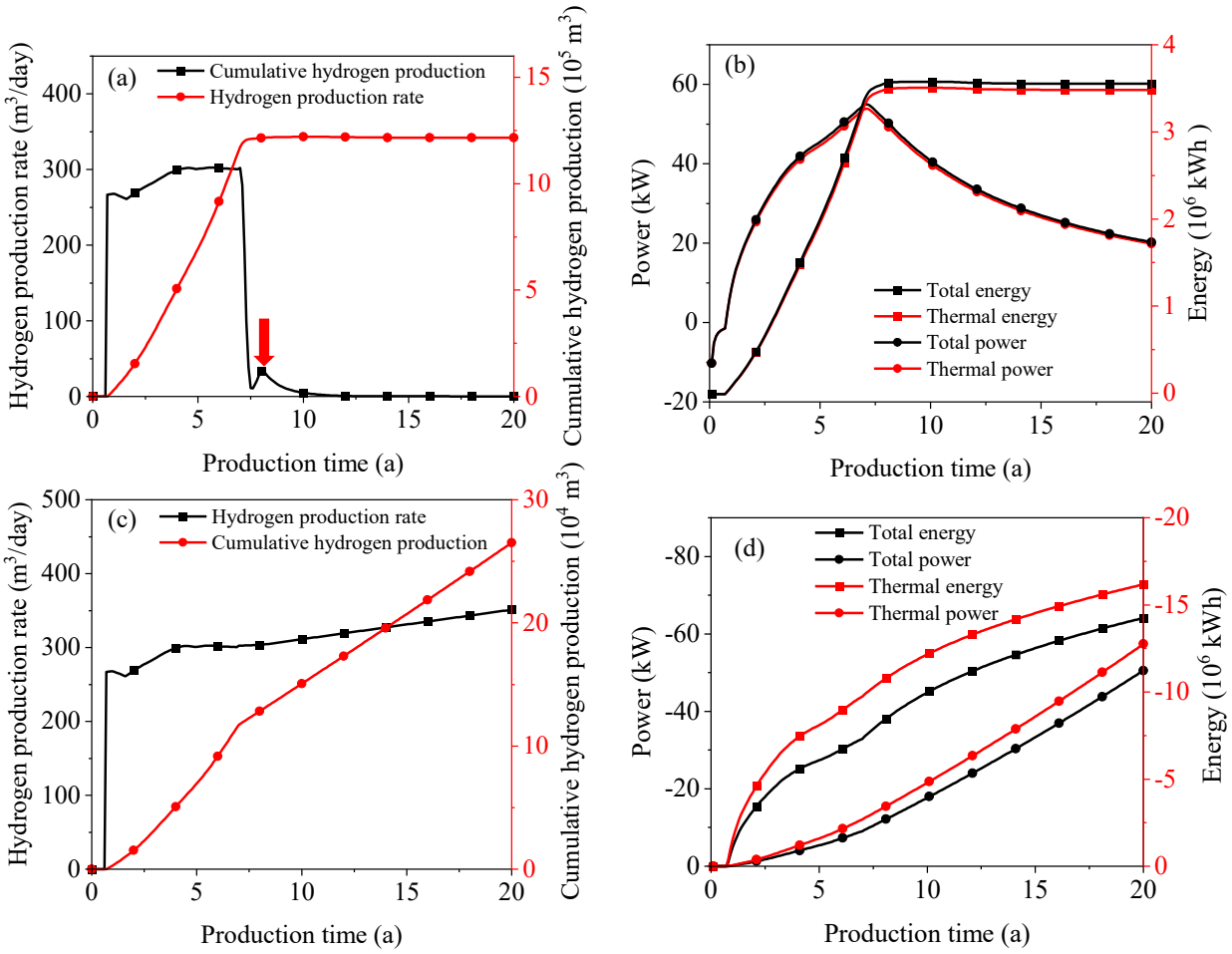


**Fig. 10**. Hydrogen production and energy output in Case 3. (a)-(b) Short-term activation and (c)-(d) continuous injection.

strategies, such as using catalysts, modifying the injected fluid chemistry, or enhancing geothermal utilization, could lower activation energy and reduce external energy requirements, thus improving hydrogen yield and system energy performance.

## 5. Parameter sensitivity analysis

Given that most actual production environments do not possess the high-temperature heated zone of Case 1, and that the economic feasibility of continuous high-temperature injection is insufficient, system performance is closer to the constrained state of Case 3. Therefore, the parameter sensitivity analysis in this study is primarily based on the short-term high-temperature activation scenario of Case 3, quantifying the influence patterns and control mechanisms of various parameters on hydrogen production and thermal energy output characteristics from the perspectives of geometric parameters and reaction kinetics.

Geometric parameters, including hydraulic fracture width and number, and well spacing, strongly influence hydrogen and thermal energy production. Increasing fracture width enhances permeability and fluid flux, boosting cumulative hydrogen production, whereas excessive width shortens fluid residence time, slowing hydrogen production rate (Fig. 11(a)) and reducing thermal energy recovery (Fig. 11(b)). The hydrogen production rate is mainly controlled by reaction kinetics rather than fracture width. Increasing the number of fractures expands the water-rock contact and improves fluid distribution, enhancing cumulative hydrogen production (Fig. 11(c)). However, too many fractures cause fluid competition and reduce reaction efficiency, leading to lower cumulative hydrogen and thermal output (Fig. 11(d)). Wider well spacing increases the rock volume participating in serpentinization, raising cumulative hydrogen production (Fig. 11(e)). Initially, this reduces fluid flow and system power, but over time, longer fluid residence promotes thermal recovery and increases hydrogen energy output (Fig. 11(f)).

The serpentinization kinetic parameter A represents the overall reaction intensity of the system, integrating effects of catalysts, fluid chemistry, and engineering measures. Studies have shown that adding 1 wt% $Ni^{2+}$ can reduce activation energy and increase serpentinization rate by nearly two orders of magnitude, while $Al^{3+}$ and $Cr^{3+}$ can enhance the rate by 8%-20%. Acidic environments increase peridotite dissolution, maintaining high reaction rates, whereas alkaline conditions promote $Fe^{2+}$ oxidation, sustaining hydrogen generation. As shown in Fig. 12, increasing *A* significantly improves cumulative hydrogen production, production rate, power, and energy output. The sensitivity of *A* is higher than that of geometric

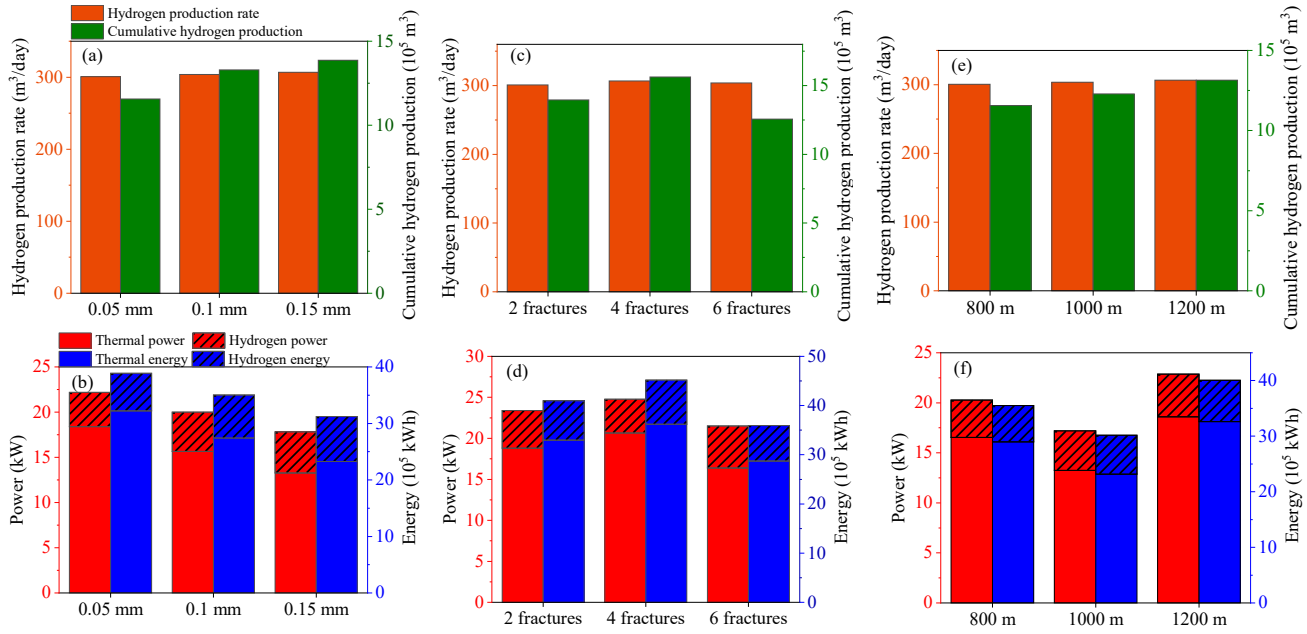


**Fig. 11**. Effects of geometric parameters on hydrogen production and energy output over 20 years. (a)-(b) Fracture width, (c)-(d) number of fractures and (e)-(f) well spacing.

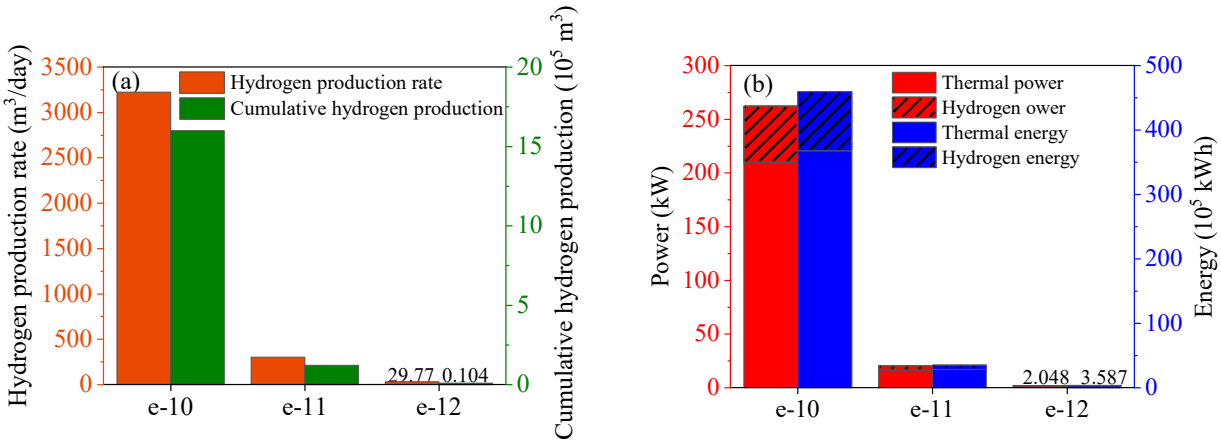


**Fig. 12**. Effects of kinetic parameter on hydrogen production and energy output over 20 years. (a) Hydrogen production rate and cumulative hydrogen production and (b) power and energy output.

fracture or well pattern parameters. A low $A$ value ($10^{-12}$ $s^{-1}$) shows kinetic lag, while high values ($10^{-10}$ $s^{-1}$) rapidly enter the acceleration stage, achieving high hydrogen production in a short time (Fig. 12(a)). Enhanced A also increases reaction heat release, improving fluid heat content and boosting both hydrogen and thermal energy output (Fig. 12(b)).

From an engineering design perspective, these sensitivity parameters can be further divided into controllable operational or stimulation parameters and geology-constrained parameters. The hydraulic fracture width and number are mainly controlled by the hydraulic stimulation design, including injection pressure, fluid volume, proppant placement, and fracturing stage arrangement. The kinetic parameter $A$ can also be partially regulated through engineering measures, including catalyst addition, fluid chemistry adjustment, and pH control. In contrast, well spacing is constrained by reservoir scale, drilling conditions, and field layout, although it can still be optimized during well-pattern design. Formation temperature, in-situ stress, and natural fracture development are primarily governed by geological conditions and are difficult to actively control in the field. Therefore, the sensitivity analysis highlights that field optimization should mainly focus on controllable parameters, such as fracture geometry and reaction-kinetic enhancement, while geological parameters should be used as boundary conditions for site selection and feasibility evaluation.

## 6. Challenges and perspectives

Although the dual horizontal well hydraulic fracturing scheme provides a potentially effective framework for stimulating serpentinization-driven hydrogen generation in peridotite, several key challenges still limit its engineering in real scenarios and large-scale applicability. The first challenge is

the limited effective reaction volume. Even after hydraulic stimulation, only a fraction of the rock mass can be accessed by injected water, and the actual reactive surface area remains far smaller than the geometric reservoir volume. More importantly, the present concept depends strongly on maintaining a favorable thermal window for serpentinization. In practical reservoirs, however, the thermal regime is dynamic rather than idealized: The temperature of the active reaction zone may be reduced by wellbore heat loss, mixing between injected and formation fluids, local cooling near the injection end, and progressive depletion of accessible heat . Therefore, thermal realism must be regarded as a first-order constraint rather than a secondary issue, particularly in low-geothermal settings where the reaction may not be self-sustaining.

A second challenge is the limitation imposed by system-level energy balance. The artificial stimulation of serpentinization is not governed solely by hydrogen generation potential but also by the energy required to heat injected water, sustain circulation, overcome pumping losses, and manage hydrogen production and separation at the surface. If these external energy inputs are not explicitly considered, the apparent benefit of hydrogen generation may be overstated. This issue is especially important for reservoirs with insufficient geothermal support, where continuous high-temperature injection may lead to marginal or even negative net energy output. Thus, any engineering assessment must move beyond hydrogen yield alone and evaluate the net energy performance of the full coupled system.

A third challenge is that hydrogen generation and transport are inherently multiphase processes. As serpentinization progresses, dissolved $H_2$ may exceed its solubility limit and exsolve into a free gas phase. The appearance of gas saturation can alter relative permeability, capillary pressure, and effective water mobility, thereby reducing water replenishment into reactive regions and weakening the water-rock contact. At the same time, exsolved hydrogen may undergo dissolution, re-dissolution, buoyancy-driven segregation, local accumulation, and leakage along conductive fractures or fault zones. These processes directly affect both recoverable hydrogen and reservoir pressure evolution, yet they are not fully represented in simplified single-phase descriptions. Consequently, the predictability of hydrogen productivity, recovery efficiency and migration risk remains limited without explicitly accounting for multiphase flow and gas transport behavior.

A fourth challenge concerns the long-term evolution of the fracture-pore system and the uncertainty associated with scale-up. The fracture network formed by hydraulic fractures and natural fractures is difficult to characterize accurately in terms of geometry, connectivity, aperture distribution, and stimulated reservoir volume. Meanwhile, serpentinization continuously modifies reservoir structure through mineral dissolution, secondary mineral precipitation, solid-volume expansion, and gas-pressure buildup. These coupled processes may either enhance connectivity through reaction-induced cracking or reduce injectivity through pore and fracture clogging, leading to strongly nonlinear evolution of porosity and permeability over time. When such local-scale uncertainties are extrapolated to the field scale, additional uncertainty arises from spatial heterogeneity, operational variability and the incomplete knowledge of boundary conditions. In view of these limitations, future research should focus on four priorities: (1) Improving the reaction efficiency by regulating the chemical environment of the injected fluid, including pH, redox state, catalytic additives, electrical stimulation, and possibly microbial mediation; (2) strengthening multi-scale fracture characterization and modeling to better constrain the spatial extent of water flow, heat transfer, and reaction zones; (3) advancing reservoir simulation from thermo-hydro-chemical toward thermo-hydro-mechanical-chemical frameworks that incorporate mineral expansion, precipitation-induced blockage, gas exsolution, capillary effects, and pressure feedback from hydrogen accumulation; and (4) explicitly integrating full energy-balance analysis, uncertainty quantification, and field-scale upscaling into engineering evaluation. Only by addressing these issues together can the practical feasibility of artificially stimulated serpentinization hydrogen generation in peridotite be assessed more realistically.

## 7. Conclusions

To overcome the constraints on natural hydrogen generation, migration and accumulation, this study develops a THC coupled model to simulate water injection-induced serpentinization in peridotite formations through dual horizontal well fracturing, enabling in-situ hydrogen generation and direct recovery. The main conclusions are summarized as follows:

1) Under high geothermal temperature conditions, high-temperature injection significantly enhances serpentinization kinetics. In the 20-year production period, the presence of natural fractures increases cumulative hydrogen production by nearly one order of magnitude compared with the non-fractured conditions, and the peak hydrogen production rate reaches 4,300 $m^3$/d, demonstrating the potential for sustained high-level hydrogen production.
2) Low-temperature injection under high geothermal temperature conditions significantly inhibits serpentinization kinetics, reducing the reaction rate by about 80% and decreasing cumulative hydrogen production by nearly 85% compared with high-temperature injection. In this scenario, system energy output is dominated by geothermal energy. As the injection temperature increases, hydrogen and heat production rise simultaneously; however, an optimal temperature range (230-310 °C) is identified.
3) Under normal geothermal temperature conditions, high-temperature activation significantly accelerates serpentinization in the early stage, but the thermal influence is spatially limited and the reservoir heat dissipates rapidly, constraining hydrogen productivity. Continuous high-temperature injection can maintain moderate hydrogen output, yet the system exhibits strong dependence on external heat input, necessitating engineering enhancement measures for sustainable operation.
4) The hydrogen and heat production capacities exhibit distinct sensitivities to the engineering parameters. Appropriately increasing the hydraulic fracture width promotes hydrogen generation, whereas heat recovery is more sen-

sitive to well spacing. In addition, optimizing the number of hydraulic fractures enhances both hydrogen and heat production to varying degrees. Overall, strengthening the reaction kinetics is the key factor governing the hydrogen generation capacity of the system.

Overall, this work should be regarded as a first-order conceptual modeling study rather than a predictive field-scale engineering assessment. The results are conditioned by several idealized assumptions, including a constant geothermal heat source, fixed permeability, simplified reaction kinetics, and single-phase flow behavior. Future work should therefore incorporate fracture evolution, variable permeability, and multiphase hydrogen migration to more rigorously evaluate field-scale feasibility.

## Acknowledgements

We would like to express our appreciation to the following institutions for their funding support: The 2025 Postdoctoral Innovative Talent Support Program, "Study on the Mechanism of Spontaneous Fracturing and Permeability Enhancement in Peridotite Induced by Hydrogen-Generating Reactions" (No. BX20250029); the 2024 Frontier Interdisciplinary Exploration Research Program of China University of Petroleum, Beijing, "Natural Hydrogen Generation and Migration in Peridotite under Multi-Scale Fracturing Mechanisms" (No. 2462024XKQY002), and the Natural Science Foundation of Xinjiang Uygur Autonomous Region, "Natural Hydrogen Generation and Migration Mechanisms in Peridotite under Spontaneous Fracturing" (No. 2025D01B202).

## Conflicts of interest

The authors declare no competing interest.



## References

Abidoye, L. K., Khudaida, K. J., Das, D. B. Geological carbon sequestration in the context of two-phase flow in porous media: A review. Critical Reviews in Environmental Science and Technology, 2015, 45(11): 1105-1147.

Albers, E., Bach, W., Pérez-Gussinyé, M., et al. Serpentinization-driven $H_2$ production from continental break-up to mid-ocean ridge spreading: Unexpected high rates at the West Iberia margin. Frontiers in Earth Science, 2021, 9: 673063.

Aliyu, M. D., Archer, R. A. A thermo-hydro-mechanical model of a hot dry rock geothermal reservoir. Renewable Energy, 2021, 176: 475-493.

Allen, D. E., Seyfried, W. E. Serpentinization and heat generation: Constraints from Lost City and Rainbow hydrothermal systems. Geochimica et Cosmochimica Acta, 2004, 68(6): 1347-1354.

Aquino, K. A., Perez, A. dC., Juego, C. M. M., et al. High hydrogen outgassing from an ophiolite-hosted seep in Zambales, Philippines. International Journal of Hydrogen Energy, 2025, 105: 360-366.

Arekhov, V., Zhainakov, T., Clemens, T., et al. Influence of water saturation, temperature and pressure on the effective hydrogen-methane gas diffusion in reservoir rocks. Paper SPE 220008 Presented at SPE Europe Energy Conference and Exhibition, Turin, Italy, 26-28 June, 2024.

Boon, M., Rademaker, T., Winardhi, C. W., et al. Multiscale experimental study of $H_2$/brine multiphase flow in porous rock characterizing relative permeability hysteresis, hydrogen dissolution, and Ostwald ripening. Scientific Reports, 2024, 14(1): 30170.

Brandt, A. R. Greenhouse gas intensity of natural hydrogen produced from subsurface geologic accumulations. Joule, 2023, 7(8): 1818-1831.

Cao, J., Zhang, N., James, L. A., et al. Modeling semi-steady state near-well flow performance for horizontal wells in anisotropic reservoirs. Computational Geosciences, 2018, 22(3): 725-744.

Davies, R. J., Mathias, S. A., Moss, J., et al. Hydraulic fractures: How far can they go? Marine and Petroleum Geology, 2012, 37(1): 1-6.

Egert, R., Neupane, G., Jin, W. On the viability of stimulated hydrogen generation from iron-rich formations. Geoenergy Science and Engineering, 2026, 256: 214130.

Emmanuel, S., Berkowitz, B. Suppression and stimulation of seafloor hydrothermal convection by exothermic mineral hydration. Earth and Planetary Science Letters, 2006, 243(3-4): 657-668.

Flude, S., Warr, O., Magalhães, N., et al. Generation, migration and accumulation of natural hydrogen and helium in the intracratonic São Francisco Basin, eastern Brazil: Implications for the understanding and exploration of natural $H_2$ systems. Geoenergy, 2025, 3(1): geoenergy2024-042.

Foustoukos, D. I., Seyfried, W. E. Hydrocarbons in hydrothermal vent fluids: The role of chromium-bearing catalysts. Science, 2004, 304(5673): 1002-1005.

Frost, B. R., Beard, J. S. On silica activity and serpentinization. Journal of Petrology, 2007, 48(7): 1351-1368.

Gabriel, K. S., El-Emam, R. S., Zamfirescu, C. Technoeconomics of large-scale clean hydrogen production - A review. International Journal of Hydrogen Energy, 2022, 47(72): 30788-30798.

Hatakeyama, K., Katayama, I., Hirauchi, K., et al. Mantle hydration along outer-rise faults inferred from serpentinite permeability. Scientific Reports, 2017, 7(1): 13870.

Hsieh, J. C., Li, B. H., Lee, B. H., et al. Performance and economic analyses of a geothermal reservoir model coupled with a flash-binary cycle model. Renewable Energy, 2024, 230: 120826.

Huang, R., Song, M., Ding, X., et al. Influence of pyroxene and spinel on the kinetics of peridotite serpentinization. Journal of Geophysical Research: Solid Earth, 2017, 122(9): 7111-7126.

Ingersoll, L. R., Zobel, O. J., Ingersoll, A. C. Heat conduction with engineering, geological, and other applications. Physics Today, 1955, 8(3): 17.

Jackson, O., Lawrence, S. R., Hutchinson, I. P., et al. Nat-

ural hydrogen: Sources, systems and exploration plays. Geoenergy, 2024, 2(1): geoenergy2024-002.

Kelley, D. S., Karson, J. A., Früh-Green, G. L., et al. A serpentinite-hosted ecosystem: The Lost City hydrothermal field. Science, 2005, 307(5714): 1428-1434.

Kottwitz, M. O., Popov, A. A., Baumann, T. S., et al. The hydraulic efficiency of single fractures: Correcting the cubic law parameterization for self-affine surface roughness and fracture closure. Solid Earth, 2020, 11(3): 947-957.

Li, T., Shiozawa, S., McClure, M. W. Thermal breakthrough calculations to optimize design of a multiple-stage enhanced geothermal system. Geothermics, 2016, 64: 455-465.

Liu, J., Wang, S., Javadpour, F., et al. Hydrogen diffusion in clay slit: Implications for the geological storage. Energy & Fuels, 2022, 36(14): 7651-7660.

Liu, J., Wolterbeek, T. K. T., Spiers, C. J. Volumetric response and permeability evolution during carbonation of crushed peridotite under controlled stress-pressure-temperature conditions. International Journal of Rock Mechanics and Mining Sciences, 2024, 182: 105886.

Lollar, B. S., Onstott, T. C., Lacrampe-Couloume, G., et al. The contribution of the Precambrian continental lithosphere to global $H_2$ production. Nature, 2014, 516(7531): 379-382.

Luhmann, A. J., Tutolo, B. M., Bagley, B. C., et al. Chemical and physical changes during seawater flow through intact dunite cores: An experimental study at 150-200 °C. Geochimica et Cosmochimica Acta, 2017, 214: 86-114.

Mahmoodpour, S., Singh, M., Turan, A., et al. Simulations and global sensitivity analysis of the thermo-hydraulic-mechanical processes in a fractured geothermal reservoir. Energy, 2022, 247: 123511.

Malvoisin, B., Brunet, F. Water diffusion-transport in a synthetic dunite: Consequences for oceanic peridotite serpentinization. Earth and Planetary Science Letters, 2014, 403: 263-272.

Malvoisin, B., Brunet, F., Carlut, J., et al. Serpentinization of oceanic peridotites: 2. Kinetics and processes of San Carlos olivine hydrothermal alteration. Journal of Geophysical Research: Solid Earth, 2012, 117(B4): 2011JB008842.

Malvoisin, B., Dörfler, P., Auzende, A.-L., et al. Magnetite production in mesh texture during serpentinization, a marker of $H_2$ diffusion. Journal of Petrology, 2026, 67(4): egag021.

Manfredi, A., Manfrida, G., Carcasci, C., et al. Integration of hydrogen production with geothermal power plants: Utilizing $H_2$ as a spinning reserve unit. Renewable Energy, 2026, 256: 124630.

Mao, S., Yu, S., Xu, J., et al. Geologic hydrogen: A review of resource potential, subsurface dynamics, exploration, production, transportation, and research opportunities. Energy & Environmental Science, 2025, 18(23): 9991-10035.

Marcaillou, C., Muñoz, M., Vidal, O., et al. Mineralogical evidence for $H_2$ degassing during serpentinization at 300 °C/300 bar. Earth and Planetary Science Letters, 2011, 303(3-4): 281-290.

Martin, B., Fyfe, W. S. Some experimental and theoretical observations on the kinetics of hydration reactions with particular reference to serpentinization. Chemical Geology, 1970, 6: 185-202.

McCollom, T. M., Bach, W. Thermodynamic constraints on hydrogen generation during serpentinization of ultramafic rocks. Geochimica et Cosmochimica Acta, 2009, 73(3): 856-875.

McCollom, T. M., Klein, F., Robbins, M., et al. Temperature trends for reaction rates, hydrogen generation, and partitioning of iron during experimental serpentinization of olivine. Geochimica et Cosmochimica Acta, 2016, 181: 175-200.

McCollom, T. M., Klein, F., Solheid, P., et al. The effect of pH on rates of reaction and hydrogen generation during serpentinization. Philosophical Transactions of the Royal Society A: Mathematical, Physical and Engineering Sciences, 2020, 378(2165): 20180428.

Moretti, I., Baby, P., Alvarez Zapata, P., et al. Subduction and hydrogen release: The case of Bolivian Altiplano. Geosciences, 2023, 13(4): 109.

Mügler, C., Jean-Baptiste, P., Perez, F., et al. Modeling of hydrogen production by serpentinization in ultramafic-hosted hydrothermal systems: Application to the Rainbow field. Geofluids, 2016, 16(3): 476-489.

Nadaleti, W. C., Lourenço, V. A., Americo, G. Green hydrogen-based pathways and alternatives: Towards the renewable energy transition in South America's regions - Part A. International Journal of Hydrogen Energy, 2021, 46(43): 22247-22255.

Norbeck, J. H., McClure, M. W., Horne, R. N. Field observations at the Fenton Hill enhanced geothermal system test site support mixed-mechanism stimulation. Geothermics, 2018, 74: 135-149.

Noyan, O. F., Hasan, M. M., Pala, N. A global review of the hydrogen energy eco-system. Energies, 2023, 16(3): 1484.

Okere, C. J., Sheng, J. J. Optimizing hydrogen generation from petroleum reservoirs: A dual-perspective approach for enhancing efficiency and cleaner production. Gas Science and Engineering, 2025, 136: 205576.

Okland, I., Huang, S., Thorseth, I. H., et al. Formation of $H_2$, $CH_4$ and N-species during low-temperature experimental alteration of ultramafic rocks. Chemical Geology, 2014, 387: 22-34.

Osselin, F., Soulaine, C., Fauguerolles, C., et al. Orange hydrogen is the new green. Nature Geoscience, 2022, 15(10): 765-769.

Perez, F., Mügler, C., Jean-Baptiste, P., et al. Coupled modeling of thermics and hydrogeology with the Cast3M code: Application to the Rainbow hydrothermal field (Mid-Atlantic Ridge, 36°14'N). Computational Geosciences, 2013, 17(2): 217-237.

Prinzhofer, A., Moretti, I., Françolin, J., et al. Natural hydrogen continuous emission from sedimentary basins: The example of a Brazilian $H_2$-emitting structure. International Journal of Hydrogen Energy, 2019, 44(12): 5676-

5685.

Prinzhofer, A., Tahara Cissé, C. S., Diallo, A. B. Discovery of a large accumulation of natural hydrogen in Bourakebougou (Mali). International Journal of Hydrogen Energy, 2018, 43(42): 19315-19326.

Rezaee, R. Quantifying natural hydrogen generation rates and volumetric potential in onshore serpentinization. Geosciences, 2025, 15(3): 112.

Roumejon, S., Cannat, M., Agrinier, P., et al. Serpentinization and fluid pathways in tectonically exhumed peridotites from the Southwest Indian Ridge (62-65 E). Journal of Petrology, 2015, 56(4): 703-734.

Shimizu, H., Okamoto, A. The roles of fluid transport and surface reaction in reaction-induced fracturing, with implications for the development of mesh textures in serpentinites. Contributions to Mineralogy and Petrology, 2016, 171(8-9): 73.

Strauch, B., Pilz, P., Hierold, J., et al. Experimental simulations of hydrogen migration through potential storage rocks. International Journal of Hydrogen Energy, 2023, 48(66): 25808-25820.

Vallejo, V., Nguyen, Q., Ravikumar, A. P. Geospatial variation in carbon accounting of hydrogen production and implications for the US Inflation Reduction Act. Nature Energy, 2024, 9(12): 1571-1582.

Wang, T., Yang, Y., Peng, Y., et al. Simulation and evaluation for acid fracturing of carbonate reservoirs based on embedded discrete fracture model. Natural Gas Industry B, 2021, 8(6): 637-649.

Wang, X., Yu, Z., Sun, P., et al. Serpentinization-mediated $H_2$-generation and its genesis link to supra-subduction zone ophiolites. Earth-Science Reviews, 2026, 273: 105369.

Wang, Y., Zhou, F., Zhang, Y., et al. Numerical studies and analysis on reaction characteristics of limestone and dolomite in carbonate matrix acidizing. Geoenergy Science and Engineering, 2023, 222: 211452.

Wu, H., Zhang, J., Fu, P., et al. Inferring fracture aperture distribution at the EGS Collab Experiment 1 Testbed through a deep learning accelerated Bayesian approach. Paper SGP-TR-218 Presented at 46$^{th}$ Workshop on Geothermal Reservoir Engineering, Stanford University, Stanford, California, 15-17 February, 2021.

Zgonnik, V. The occurrence and geoscience of natural hydrogen: A comprehensive review. Earth-Science Reviews, 2020, 203: 103140.

Zgonnik, V., Beaumont, V., Larin, N., et al. Diffused flow of molecular hydrogen through the Western Hajar mountains, Northern Oman. Arabian Journal of Geosciences, 2019, 12(3): 71.

Zhang, Z., Jia, G., Ma, Z., et al. Parameter optimization and ground temperature analysis of a solar-assisted medium-deep geothermal heating system under long-term operation. Renewable Energy, 2026, 261: 125234.

Zhao, K., Li, R., Lei, H., et al. Numerical simulation of influencing factors of hydraulic fracture network development in reservoirs with pre-existing fractures. Processes, 2022, 10(4): 773.